MoST-IG: Morphology-Guided Spatial Transcriptomics Integration via Visual-Genomic Graph Optimal Transport

Liting Yu*, Tao Ma*, Weiqin Zhao, Zhuo Liang, and Lequan Yu✉

The University of Hong Kong, Hong Kong SAR, China
{lityu, u3011706}@connect.hku.hk, lqyu@hku.hk

Abstract. Spatial transcriptomics (ST) is crucial for understanding cellular heterogeneity and tissue organization. However, integrating spatial transcriptomics across multiple slices remains challenging for downstream analyses, as ST slices may exhibit significant batch effects. Current methods mostly depend on forced integration via contrastive learning, which may ignore the inherent biological heterogeneity, thus impacting the performance of downstream analyses. To address these challenges, we introduce ***MoST-IG***, a multimodal framework for morphology-guided multi-slice ST integration. MoST-IG comprises two key components: (1) Cross-modal alignment between histology prior and ST. We integrate histological patterns derived from the pathological foundation model with ST using our proposed Visual-Genomic Graph Optimal Transport (VG-GOT) module. This visual-genomic alignment preserves biological heterogeneity through morphology-guided regularization while enriching the spatial context of ST data with morphological features to provide a more discriminative representation and enhance downstream performance. (2) Integration of Multi ST-Slices. A multi ST-slices Contrastive Learning (mST-CL) module is designed via two complementary triplet losses—one for both inter-slice and intra-slice cell type mapping. Experiments show that MoST-IG outperforms leading methods in both cancer grading and detection, as well as tissue structure clustering, while better preserving tissue landmarks in multi-slice ST integration. The code is available at https://github.com/HKU-MedAI/MoST-IG.

Keywords: Spatial Transcriptomics · Data Integration · Histology Imaging · Graph Optimal Transport.

1 Introduction

Spatial transcriptomics (ST) has revolutionized biological research by enabling gene expression profiling while preserving spatial context, offering unprecedented insights into tissue heterogeneity and disease mechanisms [1,2]. Integrating multiple spatial transcriptomics (ST) slices is challenging due to batch effects, which are random biases introduced by technical factors during the gene sequencing

* L. Yu and T. Ma: Contributed equally to this work.

process. These biases can stem from variations in reverse transcriptase enzyme efficiency and inconsistencies in other stages of the sequencing protocol. These factors can lead to non-biological variations between data from different batches that obscure biological signals [3,4,5]. Many existing integration methods [6,7,8] focus on learning shared latent embeddings for multiple spatial transcriptomics (ST) slices. However, most of these methods fail to consider an essential anatomical resource: the rich morphological patterns found in histology images that provide insight into high-resolution tissue architecture. This oversight is crucial because prior studies indicate that histological features can capture semantic relationships between ST spots that extend beyond mere physical proximity [9,10]. The limited use of morphological semantics in current approaches significantly hinders the ability to achieve biologically meaningful integration across ST slices, as the absence of anatomical constraints might lead to *over-mixing*. When over-mixing occurs, different slices are forcibly integrated, erasing valuable differences such as the differential expression of distinct cell types. As a result, critical spatial and molecular patterns essential for understanding tissue heterogeneity are obscured after integration.

We are the first to identify and balance the twin pitfalls of over-mixing (obscuring biological heterogeneity) and under-mixing (failing to remove batch effects) in multi-slice ST integration, and propose **Mo**rphology-guided **S**patial **T**ranscriptomics **I**nte**G**ration (***MoST-IG***, Fig. 1) to explicitly leverage histological morphology guidance. For Visual-Genomics Graph Optimal Transport (**VG-GOT**), the benefits of our cross-modal visual guidance are twofold: First, histology images act as anatomical constraints, preventing over-mixing among different ST slices by preserving distinct cell-type differences during integration. Second, histology images capture spatial organization and biological meaning in each ST slice—such as tissue zonation and cellular neighborhoods—which are not present in ST data. Incorporating these features improves the identification of hidden tissue structures beyond just molecular profiles. Specifically, MoST-IG first extracts histology image features using a pathology foundation model to serve as visual histological guidance. Then, two modality-specific graphs are constructed for each slice: a histology graph based on the extracted guidance and a gene expression graph based on ST spot embeddings. The VG-GOT module is designed to align these two modality graphs at both node feature distribution level and graph topology level [11]. In addition, to prevent under-mixing we incorporate the multi ST-slices Contrastive Learning (**mST-CL**) module to enhance the slice genomic integration, which uses two complementary triplet losses—one for inter-slice cell type mapping and another for intra-slice cell type mapping.

In summary, our key contributions are as follows: (1) We propose MoST-IG, a novel multimodal framework for multiple ST slice integration, by cross-modal visual-genomic guidance and multi ST-slices Contrastive Learning to balance over- and under-mixing. (2) We developed a Visual-Genomic Graph Optimal Transport module that effectively aligns histology image and ST. By utilizing knowledge from visual priors at both the node level and the graph topology

level, this visual-genomic alignment prevents over-mixing during ST integration, which helps preserve biological patterns more accurately, thus resulting in improved performance for downstream applications. (3) State-of-the-art (SOTA) performance across cancer grading and tissue clustering tasks with absolute improvements up to 0.183 (in ARI of prostate cancer grading) over previous best methods. Our MoST-IG successfully preserves biological patterns, both demonstrating discriminative separation of cells while removing technical variations and mapping identical cell types from different slices together.

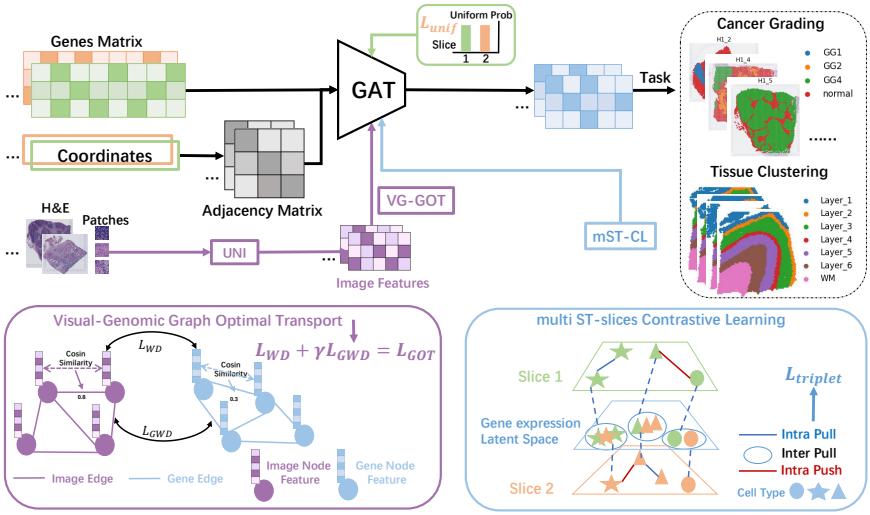

Fig. 1. MoST-IG: A Visual-Genomic framework to learn multi ST-Slices integrated representation for downstream Tasks (cancer grading and tissue clustering). The framework processes multi ST-Slices (gene expression matrices + spatial coordinates) via GAT to generate integrated representations, enhanced by: VG-GOT (purple), mST-CL (blue), and Batch-Uniform Discriminator (green).

2 Method

We present MoST-IG (Fig. 1), an innovative multimodal framework designed to learn biologically relevant, spatially aware representations across multiple ST-Slices. It maintains biological diversity while removing technical biases, facilitating the integration of various ST-Slices and enhancing spatial domain identification. Unlike previous methods, MoST-IG incorporates morphology knowledge to guide the ST integration process. Specifically, MoST-IG consists of two main components: 1) genomic integration of multi ST-slices via Contrastive Learning, and 2) Visual-Genomic alignment between histological morphology guidance and the corresponding ST data.

2.1 Multi ST-slices Contrastive Learning

To integrate the genomic expression from different ST slices, we propose a multi ST-slices Contrastive Learning (**mST-CL**) module. In this stage, we process multi ST-slices, including gene expression matrices $X \in \mathbb{R}^{N \times d_1}$ (where N is the number of spots and d_1 is the number of genes) and spatial coordinates $C \in \mathbb{R}^{N \times 2}$, through a Graph Attention Network (GAT) based encoder E_ψ. Then, the core integration is driven by two complementary triplet losses. For **inter-slice integration**, we construct cross-slice triplets using mutual nearest neighbors (MNNs) [5]: given anchor spot x^A_{anc} in slice A, we identify its positive MNN x^B_{pos} in slice B based on transcriptomic similarity, and sample a negative spot x^A_{neg} from A. The inter-slice triplet loss minimizes the embedding distance between anchors and cross-slice positives while maximizing the separation of intra-slice negatives. With $d(\cdot)$ as Euclidean distance, $z = E_\psi(x)$ and γ representing the margin, the inter-slice loss can be denoted as follows:

$$\mathcal{L}_{\text{inter}} = \max\left(d(z^A_{anc}, z^B_{pos}) - d(z^A_{anc}, z^A_{neg}) + \gamma, 0\right). \tag{1}$$

For **intra-slice disentanglement**, we design an intra-slice loss enhances biological heterogeneity within individual slices:

$$\mathcal{L}_{\text{intra}} = \sum_{x_i \in X} \max\left(d(z_i, z_{nn}) - d(z_i, z_{neg}) + \gamma, 0\right), \tag{2}$$

where z_{nn} denotes the nearest transcriptomic neighbor in the same slice and z_{neg} denotes a randomly sampled negative example. Additionally, to unify the latent space for the integrated embeddings and encourage spots to be indistinguishable across K slices, we use a pre-trained MLP discriminator D_ϕ through KL divergence minimization:

$$\mathcal{L}_{\text{unif}} = D_{KL}\left(D_\phi(z) \| \mathcal{U}\left(\frac{1}{K}\right)\right), \tag{3}$$

where $\mathcal{U}$ represents the uniform distribution over slices.

2.2 Visual-Genomic Graph Optimal Transport

To achieve morphology semantic enrichment and guided regularization, we designed a Visual-Genomic Graph Optimal Transport (**VG-GOT**) module, which aligns visual histological patterns with genomic transcriptomic profiles.

Modality-specific Graph Construction. For each pair of co-registered H&E and ST slices, we construct modality-specific graphs in the feature space: the Histology Graph $\mathcal{G}_h$ based on morphology features, and the Gene Expression Graph $\mathcal{G}_g$ based on spot features. The morphology features are extracted from H&E patches using UNI [12], while the spot features are obtained from the GAT-based encoder designed for ST representation learning. An edge is built between two nodes (j, j') in a same graph if the cosine similarity between node features $\cos(v_j, v_{j'}) > \tau_h$, where threshold $\tau_h = \min(\cos) + 0.1(\max(\cos) - \min(\cos))$ is dynamically constructed [13].

Two-level Alignment via VG-GOT. We first match the spot distributions of H&E $\hat{p}_H$ and gene expression embeddings $\hat{p}_G$ through optimal transport at the **node level**. Denoting $T \in \mathbb{R}_+^{N\times N}$ as the transport plan, we can minimize the Wasserstein Distance (WD) between distributions $\hat{p}_H$ and $\hat{p}_G$ by finding the optimal transport plan:

$$\mathcal{L}_{WD}(\hat{p}_H, \hat{p}_G) = \min_{\mathbf{T}} \sum_j \sum_m \mathbf{T}_{j,m} \cdot c(v_j^{\mathrm{H}}, v_m^G), \tag{4}$$

such that $\sum_j T_{j,m} = 1/N_G, \forall m$ and $\sum_m T_{j,m} = 1/N_H, \forall j$. The cost between H&E-gene embeddings $C(v_j^H, v_m^G)$ is computed with the cosine distance metric. In addition to the node level matching with $\mathcal{L}_{WD}$, we also wish to fully grasp neighbor information in morphology by **graph topology level** alignment. Specifically, we enforce structural consistency between visual-genomic graphs through Gromov-Wasserstein distance, matching the graph topology by comparing the edge distance between paired visual-genomic graphs. Denoting $\widetilde{T_e} \in \mathbb{R}_+^{N\times N}$ as the transport plan as before:

$$\mathcal{L}_{GWD}(\hat{p}_H, \hat{p}_G) = \min_{\widetilde{\mathbf{T}}} \sum_{j,j',m,m'} \widetilde{\mathbf{T}}_{j,m} \widetilde{\mathbf{T}}_{j',m'} \cdot ||c(v_j^H, v_{j'}^H) - c(v_m^G, v_{m'}^G)||), \tag{5}$$

such that $\widetilde{\mathbf{T}}$ and c are same as equation (4)

$$\mathcal{L}_{GOT} = \lambda \mathcal{L}_{WD} + (1-\lambda)\mathcal{L}_{GWD}, \tag{6}$$

where λ denotes a weighting term. This two-level mechanism ensures that matched spots not only have similar feature representations but also maintain consistent topological relationships within their respective modal graphs, aligning both local and global structural patterns across visual-genomic modalities.

3 Experimental Results

3.1 Experimental Settings

Datasets and Tasks. We evaluate our framework on four publicly available ST datasets, including two cancer tissue datasets and two healthy tissue datasets: **Prostate Cancer** [14]: Comprises 7 ST slices from a Gleason 4+3 (ISUP grade group 4) patient, featuring heterogeneous tumor grading distributions. Annotations include three cancer grades (*GG1, GG2, GG4*) and normal regions. This dataset presents challenges in resolving spatial tumor heterogeneity across multiple tissue sections. **HER2-positive Breast Tumors** [15]: Includes eight manually annotated tissue slices from eight independent patients. Each slice is annotated with three regions: *carcinoma in situ*, *invasive cancer*; and *normal region*. **Human DLPFC** [16]: Comprises four dorsolateral prefrontal cortex (DLPFC) slices from one donor. Annotations include six cortical layers (Layer 1–6) and white matter (WM). **Mouse Sagittal Brain** [17]: Includes four sagittal brain

slices from two tissue sections (anterior and posterior slices per section). We evaluate two tasks on the above datasets: **Cancer Grading/Detection**: For cancer datasets, we aim to distinguish subtle molecular differences between adjacent cancer grades/subtypes within and across slices. **Tissue Structure Clustering**: For healthy tissue datasets, the objective is to recover anatomically meaningful regions (e.g., cortical layers, WM) through unsupervised clustering.

Evaluation Metrics. To assess both intra-slice discrimination and cross-slice integration, we employ three metrics: **Adjusted Rand Index (ARI)** [18], quantifying cluster-label agreement ($\in [-1, 1]$), where 1 indicates perfect alignment with manual annotated labels. ARI evaluates global clustering accuracy. **cell-type local inverse Simpson's Index (cLISI)** [19], assessing local neighborhood purity ($\in [1, N_{celltype}]$). Optimal integration achieves cLISI ≈ 1, indicating that at least 50% of spots have neighborhoods containing only spots with the same label. $\mathbf{ASW_{type}}$, representing batch-corrected clustering of identical labeled spots across slices ($\in [0, 1]$ after rescaling). Higher values indicate that 1) identical-label distances are minimized across slices, and 2) different-label distances are maximized. This directly evaluates cross-slice integration quality.

Experimental details. Our method maintains excellent scalability. During training, we run VG-GOT on a random mini-batch of 2,048 nodes each epoch; during inference, OT is not recomputed. With this strategy, the large dataset ($> 20K$ spots) is trained in 10 mins, and uses only 3 GB of VRAM during test, far faster than SPIRAL [8] (several hours) and without the out-of-memory failures encountered by DeepST [7].

3.2 Comparison with State-of-the-art Methods

We comprehensively evaluate MoST-IG against four ST clustering methods: SpaGCN [20], DeepST [7], STAligner [6], and SPIRAL [8]. As demonstrated in Table 1 and Table 2 , our method achieves superior performance across all evaluation metrics (ARI, cLISI, and $\mathrm{ASW_{type}}$) on both cancer grading/detection and healthy tissue structure clustering tasks.

Cancer Grading/Detection. For cancer grading/detection tasks (Table 1), SpaGCN exhibits the lowest performance (Prostate ARI: 0.023, Breast ARI: 0.080) due to its single-slice design, which fails to address the multi-slice scenario. In contrast, integration-focused methods, SPIRAL and STAligner, achieve improved performance. Specifically, STAligner enhances cell-type separation through triplet contrastive learning (Prostate cLISI: 1.03 vs. SPIRAL's 1.06), while SPIRAL demonstrates superior cross-slice integration via optimal transport alignment (Breast $\mathrm{ASW_{type}}$: 49.03% vs. STAligner's 48.13%). DeepST further outperforms these methods by leveraging histology images, which encode spatial organization and biological semantics. However, its performance on the Prostate

Table 1. Cancer grading/detection results on two cancer tissue datasets.

Methods	Mor.	Prostate Cancer			Breast cancer		
		ARI	cLISI	$ASW_{type}(\%)$	ARI	cLISI	$ASW_{type}(\%)$
SpaGCN [20]	✓	0.023	1.28	44.56	0.080	1.73	45.87
DeepST [7]	✓	0.044	1.06	47.68	0.181	1.50	49.83
STAligner [6]	✗	0.192	1.03	48.12	0.163	1.56	48.13
SPIRAL [8]	✗	0.047	1.06	47.77	0.141	1.62	49.03
Ours	✓	**0.375** ↑	**1.00** ↓	**50.50** ↑	**0.226** ↑	**1.41** ↓	**50.85** ↑
w/o Mor.	✗	0.171	1.04	48.53	0.170(-0.056)	1.52	48.67

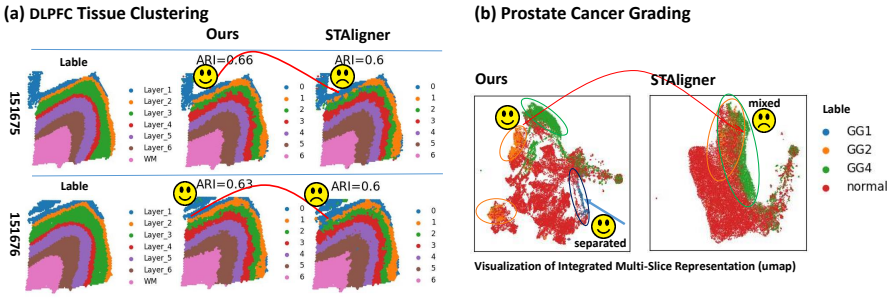

Fig. 2. **(a)** DLPFC clustering results comparison with STAligner. Ours provides a more continuous clustering of thin cortical layers (e.g., orange layer 1) compared to STAligner, thus higher ARI (clustering accuracy). **(b)** Prostate cancer grading results comparison with STAligner. UMAP visualization of learned representation: Ours illustrates clear separation consistent with labels (e.g., GG2-orange points vs. GG4-green points), while STAligner wrongly over-mixes different labeled spots.

dataset is suboptimal, as the dataset is too large for DeepST's processing pipeline, which follows a single-slice strategy. H&E staining plays a crucial role in clinical cancer diagnosis, providing important guidance for grading. Guided by this histological morphology prior, MoST-IG achieves significant performance improvements (Prostate ARI: 0.375, with a +0.183 increase; Breast ARI: 0.226, with a +0.045 increase). The UMAP visualization in Fig. 2(b) illustrates the clear separation of labeled spots after integration using our method. In contrast, STAligner fails to distinguish heterogeneity between adjacent cancer grades (e.g., GG2-orange points vs. GG4-green points) due to over-mixing, further demonstrating the effectiveness of our approach.

Healthy Tissue Structure Clustering. For healthy tissue clustering tasks (Table 2), SpaGCN, lacking an integration module, exhibits suboptimal performance. On consecutive DLPFC slices, which are anatomically similar but contain subtle cortical layer heterogeneity, STAligner achieves superior performance (ARI: 0.607, cLISI: 1.17), benefiting from its effective separation mod-

Table 2. Tissue structure clustering results on two healthy tissue datasets.

Methods	Mor.	DLPFC			Mouse Brain Sagittal		
		ARI	cLISI	ASW_{type}(%)	ARI	cLISI	ASW_{type}(%)
SpaGCN [20]	✓	0.313	2.68	39.73	0.145	1.42	27.81
DeepST [7]	✓	0.555	1.23	57.40	0.380	1.06	52.58
STAligner [6]	✗	0.607	1.17	55.64	0.369	1.26	52.42
SPIRAL [8]	✗	0.508	1.52	53.35	0.385	1.06	53.92
Ours	✓	**0.635** ↑	**1.09** ↓	**57.54** ↑	**0.401** ↑	**1.04** ↓	**54.39** ↑
w/o Mor.	✗	0.569	1.14	57.43	0.373(-0.028)	1.23	52.95

ule based on Triplet Contrastive Learning. In contrast, SPIRAL performs better on anatomically distinct (anterior/posterior) Mouse Brain Sagittal sections (ARI: 0.385, ASW_{type}: 53.92%), leveraging robust Optimal Transport for cross-slice mapping. DeepST achieves intermediate performance between these two approaches (DLPFC ARI: 0.555, Sagittal ARI: 0.380), indicating that incorporating H&E morphological information can enhance clustering to a certain extent. Our method establishes new state-of-the-art performance across all scenarios, achieving the highest clustering accuracy (DLPFC ARI: 0.635, Sagittal ARI: 0.401). The clustering visualization (Fig. 2(a)) compares our method with STAligner on DLPFC. Our approach provides a clearer and more continuous representation of thin cortical layers compared to STAligner, particularly in distinguishing layer 1 (orange layer) from layer 2 (green layer), further demonstrating its effectiveness.

3.3 Ablation Study

To assess the effectiveness of our morphology-guided approach, we perform ablation studies by removing histological morphology guidance (w/o Mor) and report the results in the last row of Table 1 and Table 2. The absence of morphology guidance leads to a significant performance drop in both cancer grading/detection (up to a 0.204 decrease in ARI for prostate cancer grading) and tissue structure clustering (up to a 0.066 decrease in ARI for DLPFC clustering). These results highlight the critical role of morphological information in capturing essential pathological features for cancer grading/detection and in preserving spatial patterns for tissue clustering. Furthermore, we observe that the performance degradation is more pronounced in cancer-related tasks, emphasizing the importance of morphological priors in improving accuracy for cancer diagnosis and classification.

4 Conclusion

In this study, we propose MoST-IG, a novel multimodal framework for integrating ST across multiple slices. By combining multi ST-slices contrastive inte-

gration and visual-genomic Graph optimal transport alignment, MoST-IG effectively integrates multi ST-slices and balance under- and over-mixing, mapping identical cell types from different slices together while preserving biological heterogeneity. The learned representation is robust for downstream ST analyses, thereby enhancing the reliability and accuracy of biological tasks.

Acknowledgments. This work was supported in part by the Research Grants Council of Hong Kong (27206123, C5055-24G, and T45-401/22-N), the Hong Kong Innovation and Technology Fund (ITS/273/22, ITS/274/22, and GHP/318/22GD), the National Natural Science Foundation of China (No. 62201483), and Guangdong Natural Science Fund (No. 2024A1515011875).

Disclosure of Interests. The authors have no competing interests to declare that are relevant to the content of this article.

References

1. Vivien Marx. Method of the year: spatially resolved transcriptomics. *Nature methods*, 18(1):9–14, 2021.
2. Luyi Tian, Fei Chen, and Evan Z Macosko. The expanding vistas of spatial transcriptomics. *Nature Biotechnology*, 41(6):773–782, 2023.
3. Shuangsang Fang, Bichao Chen, Yong Zhang, Haixi Sun, Longqi Liu, Shiping Liu, Yuxiang Li, and Xun Xu. Computational approaches and challenges in spatial transcriptomics. *Genomics, Proteomics & Bioinformatics*, 21(1):24–47, 2023.
4. Jeffrey T Leek, Robert B Scharpf, Héctor Corrada Bravo, David Simcha, Benjamin Langmead, W Evan Johnson, Donald Geman, Keith Baggerly, and Rafael A Irizarry. Tackling the widespread and critical impact of batch effects in high-throughput data. *Nature Reviews Genetics*, 11(10):733–739, 2010.
5. Laleh Haghverdi, Aaron TL Lun, Michael D Morgan, and John C Marioni. Batch effects in single-cell rna-sequencing data are corrected by matching mutual nearest neighbors. *Nature biotechnology*, 36(5):421–427, 2018.
6. Xiang Zhou, Kangning Dong, and Shihua Zhang. Integrating spatial transcriptomics data across different conditions, technologies and developmental stages. *Nature Computational Science*, 3(10):894–906, 2023.
7. Chang Xu, Xiyun Jin, Songren Wei, Pingping Wang, Meng Luo, Zhaochun Xu, Wenyi Yang, Yideng Cai, Lixing Xiao, Xiaoyu Lin, et al. Deepst: identifying spatial domains in spatial transcriptomics by deep learning. *Nucleic Acids Research*, 50(22):e131–e131, 2022.
8. Tiantian Guo, Zhiyuan Yuan, Yan Pan, Jiakang Wang, Fengling Chen, Michael Q Zhang, and Xiangyu Li. Spiral: integrating and aligning spatially resolved transcriptomics data across different experiments, conditions, and technologies. *Genome Biology*, 24(1):241, 2023.
9. Bryan He, Ludvig Bergenstråhle, Linnea Stenbeck, Abubakar Abid, Alma Andersson, Åke Borg, Jonas Maaskola, Joakim Lundeberg, and James Zou. Integrating spatial gene expression and breast tumour morphology via deep learning. *Nature biomedical engineering*, 4(8):827–834, 2020.
10. Weiqin Zhao, Zhuo Liang, Xianjie Huang, Yuanhua Huang, and Lequan Yu. Hist2cell: Deciphering fine-grained cellular architectures from histology images. *bioRxiv*, pages 2024–02, 2024.

11. Liqun Chen, Zhe Gan, Yu Cheng, Linjie Li, Lawrence Carin, and Jingjing Liu. Graph optimal transport for cross-domain alignment. In *International Conference on Machine Learning*, pages 1542–1553. PMLR, 2020.
12. Richard J Chen, Tong Ding, Ming Y Lu, Drew FK Williamson, Guillaume Jaume, Andrew H Song, Bowen Chen, Andrew Zhang, Daniel Shao, Muhammad Shaban, et al. Towards a general-purpose foundation model for computational pathology. *Nature Medicine*, 30(3):850–862, 2024.
13. Guillaume Jaume, Anurag Vaidya, Andrew Zhang, Andrew H. Song, Richard J. Chen, Sharifa Sahai, Dandan Mo, Emilio Madrigal, Long Phi Le, and Faisal Mahmood. Multistain pretraining for slide representation learning in pathology. In *European Conference on Computer Vision*, pages 19–37. Springer, 2024.
14. Andrew Erickson, Mengxiao He, Emelie Berglund, Maja Marklund, Reza Mirzazadeh, Niklas Schultz, Linda Kvastad, Alma Andersson, Ludvig Bergenstråhle, Joseph Bergenstråhle, et al. Spatially resolved clonal copy number alterations in benign and malignant tissue. *Nature*, 608(7922):360–367, 2022.
15. Alma Andersson, Ludvig Larsson, Linnea Stenbeck, Fredrik Salmén, Anna Ehinger, Sunny Wu, Ghamdan Al-Eryani, Daniel Roden, Alex Swarbrick, Åke Borg, et al. Spatial deconvolution of her2-positive breast tumors reveals novel intercellular relationships. *bioRxiv*, pages 2020–07, 2020.
16. Kristen R Maynard, Leonardo Collado-Torres, Lukas M Weber, Cedric Uytingco, Brianna K Barry, Stephen R Williams, Joseph L Catallini, Matthew N Tran, Zachary Besich, Madhavi Tippani, et al. Transcriptome-scale spatial gene expression in the human dorsolateral prefrontal cortex. *Nature neuroscience*, 24(3):425–436, 2021.
17. `https://www.10xgenomics.com/datasets/mouse-brain-serial-section-2-sagittal-anterior-1-standard`.
18. Fabian Pedregosa, Gaël Varoquaux, Alexandre Gramfort, Vincent Michel, Bertrand Thirion, Olivier Grisel, Mathieu Blondel, Peter Prettenhofer, Ron Weiss, Vincent Dubourg, et al. Scikit-learn: Machine learning in python. *the Journal of machine Learning research*, 12:2825–2830, 2011.
19. Wei Liu, Xu Liao, Ziye Luo, Yi Yang, Mai Chan Lau, Yuling Jiao, Xingjie Shi, Weiwei Zhai, Hongkai Ji, Joe Yeong, et al. Probabilistic embedding, clustering, and alignment for integrating spatial transcriptomics data with precast. *Nature communications*, 14(1):296, 2023.
20. Jian Hu, Xiangjie Li, Kyle Coleman, Amelia Schroeder, Nan Ma, David J Irwin, Edward B Lee, Russell T Shinohara, and Mingyao Li. Spagcn: Integrating gene expression, spatial location and histology to identify spatial domains and spatially variable genes by graph convolutional network. *Nature methods*, 18(11):1342–1351, 2021.